PERGAMON

International Journal of Solids and Structures 36 (1999) 5453–5466

INTERNATIONAL JOURNAL OF SOLIDS and STRUCTURES

www.elsevier.com/locate/ijsolstr

Effect of large elastic strains on cavitation instability predictions for elastic–plastic solids

Viggo Tvergaard*

Department of Solid Mechanics, Technical University of Denmark, DK- 2800 *Lyngby, Denmark*

Received 26 February 1998

Abstract

For an infinite solid containing a void, the cavitation instability limit is defined as the remote stress–and strain state, at which the void grows without bound, driven by the elastic energy stored in the surrounding material. Such cavitation limits have been analysed by a number of authors for metal plasticity as well as for nonlinear elastic solids. The analyses for elastic–plastic solids are here extended to consider the effect of a large initial yield strain, and it is shown how the critical stress value decays for increasing value of the yield strain. Analyses are carried out for remote hydrostatic tension as well as for more general axisymmetric remote stress field, with an initially spherical void. Different levels of strain hardening are considered.

1. Introduction

Unstable growth of a small void in an elastic–plastic solid can occur when the stress level in the surrounding material is sufficiently high, so that the elastic energy released by the void expansion is sufficient to drive the expansion. For a cavity in an infinite elastic–plastic material under pure hydrostatic tension the critical stress was determined early on (Bishop, Hill and Mott, 1945; Hill, 1950), at which the void grows without bound, while the strain and stress states at infinity remain unchanged. Also in the context of nonlinear elasticity much interest has been devoted to the study of cavitation instabilities (Ball, 1982; Horgan and Abeyaratne, 1986; Horgan, 1992).

In tensile experiments on highly constrained ductile wires Ashby, Blunt and Bannister (1989) found cavitation failures involving only a single void, which occurred in stress states differing from pure hydrostatic tension. Therefore, Huang et al. (1991) and Tvergaard et al. (1992) analysed void growth in axisymmetric stress states, and determined the cavitation instability limits as functions of the transverse stress over axial stress ratio. These studies have been extended to consider the effect of an initially prolate or oblate spheroidal void shape on cavitation instabilities (Tvergaard

* Fax: +45 45 93 1475; e-mail: famvig@unidhp.uni-c.dk

0020-7683/99/$ - see front matter
PII: S0020-7683(98)00244-3

and Hutchinson, 1993), or the effect of interaction between different size voids at the cavitation limit (Tvergaard, 1996, 1998).

The analyses of cavitation instabilities in elastic–plastic studies mentioned above have focused on metals, and therefore the values considered for the initial yield strain in uniaxial tension, $\varepsilon_Y = \sigma_Y/E$, have been in the range relevant to most metals, i.e. 0.001–0.005. However, other materials like polymers that show an elastic–plastic type of behaviour are characterised by much higher values of the initial yield strain, even as high as 0.05–0.1. For glassy polymers with such high yield strain Steenbrink and van der Giessen (1997) have studied void growth under the spherically symmetric conditions resulting from pure hydrostatic loading. As would be expected by extrapolating the dependence of ε_Y shown in Huang et al. (1991), unstable cavity growth was found at much lower values of the critical stress, relative to the initial yield stress, than those corresponding to metals. Steenbrink et al. (1997) describe their result as an estimate, since complete convergence was not obtained in the range of initial void volume fractions analysed, and due to the fact that a visco–plastic model was used, so that the results depend on the remote strain rate applied.

The lower values of the critical cavitation stress for higher values of the initial yield strain are directly understandable from a physical point of view. The elastic stress and strain levels in the solid are approximately proportional to the yield strain, and thus the stored elastic energy per unit volume is proportional to the square of the yield strain. However, for a given increment of the void radius the corresponding plastic strain increments are rather independent of the yield strain, and therefore the dissipated plastic work per unit volume is nearly proportional to the yield strain. Accordingly, balance of plastic dissipation with released elastic energy will tend to occur at reduced stress levels for increasing initial yield strain.

The purpose of the present paper is to extend the results of Huang et al. (1991) and Tvergaard et al. (1992) for a power hardening elastic–plastic material to also cover the range of large initial yield strains. This requires an elastic–plastic material model valid for large elastic strains as well as large plastic strains. Thus, the hypoelastic approximation often used in finite strain J_2-flow theory (e.g. see Hutchinson, 1973) will not give a sufficiently accurate representation of the elastic part of the deformations, and therefore a truly elastic finite strain formulation is used here. Although the wish to consider large initial yield strains is inspired by the behaviour of the polymers, the present investigation does not make use of the special network models developed for inelastic deformation of polymers (Boyce, Parks and Argon, 1988; Arruda and Boyce, 1991; Wu and van der Giessen, 1993). The interest here is focused on classical plasticity theory, allowing for a large elastic part of the straining.

2. Material model for finite elastic strains

2.1. Deformation gradient

The position of a material point in the initial configuration, which serves as the reference configuration, is denoted by $\mathbf{x}$, relative to a fixed Cartesian frame. In the current configuration the position of the same point is denoted by $\bar{\mathbf{x}}$, and thus the displacement vector $\mathbf{u}$ and the deformation gradient $\mathbf{F}$ are defined by

$$\mathbf{u} = \bar{\mathbf{x}} - \mathbf{x}, \quad \mathbf{F} = \frac{\partial \bar{\mathbf{x}}}{\partial \mathbf{x}} \tag{2.1}$$

In formulating an elastic–plastic theory the multiplicative decomposition of the deformation gradient may be used

$$\mathbf{F} = \mathbf{F}^e \cdot \mathbf{F}^p \tag{2.2}$$

where $\mathbf{F}^p$ represents the deformation due to plasticity, while $\mathbf{F}^e$ represents the elastic deformations and any rigid body rotation (e.g. see Needleman, 1985). Now, substituting (2.2) in the expression $\dot{\mathbf{F}} \cdot \mathbf{F}^{-1}$ for the rate of deformation leads to

$$\mathbf{D} + \mathbf{W} = \dot{\mathbf{F}} \cdot \mathbf{F}^{-1} = \dot{\mathbf{F}}^e \cdot \mathbf{F}^{e-1} + \mathbf{F}^e \cdot \dot{\mathbf{F}}^p \cdot \mathbf{F}^{p-1} \cdot \mathbf{F}^{e-1} \tag{2.3}$$

where $\mathbf{D}$ is the deformation-rate tensor and $\mathbf{W}$ is the spin tensor. From (2.3) we may identify the elastic and plastic parts of these two tensors through

$$\mathbf{D}^e + \mathbf{W}^e = \dot{\mathbf{F}}^e \cdot \mathbf{F}^{e-1} \tag{2.4}$$

$$\mathbf{D}^p + \mathbf{W}^p = \mathbf{F}^e \cdot \dot{\mathbf{F}}^p \cdot \mathbf{F}^{p-1} \cdot \mathbf{F}^{e-1} \tag{2.5}$$

where $\mathbf{D} = \mathbf{D}^e + \mathbf{D}^p$ and $\mathbf{W} = \mathbf{W}^e + \mathbf{W}^p$.

As has been discussed by Needleman (1985), there is a broad class of phenomenological plasticity relations for polycrystalline solids that specify a plastic flow rule for $\mathbf{D}^p$ and take $\mathbf{W}^p \equiv \mathbf{0}$. This includes the plasticity relations in J_2 flow theory, which will be used here. It is also noted by Needleman (1985) that an elastic–plastic material model based on the relations (2.3–2.5) is fully valid for finite elastic deformations provided that a truly elastic formulation is used, for which a strain energy function exists.

2.2. Elastic constitutive relations

The constitutive relation for the elastic part of the deformations to be used here is a nonlinear elastic formulation employed by Tvergaard, Needleman and Lo (1981). This is similar to a formulation employed by Hutchinson and Neale (1978) and Hutchinson and Tvergaard (1980, 1981), and has in all cases been used as a truly elastic finite strain version of J_2 deformation theory. However, the model may be used in general as a representation of nonlinear elasticity.

The material is taken to be isotropic with the following defining relations between the principal logarithmic strains ε_i and the principal Kirchhoff stress τ_i

$$\varepsilon_i = \frac{1+\nu}{E}\tau_i - \frac{\nu}{E}(\tau_1+\tau_2+\tau_3) + \frac{3}{2}\left(\frac{1}{E_s} - \frac{1}{E}\right)\left[\tau_i - \frac{1}{3}(\tau_1+\tau_2+\tau_3)\right]. \tag{2.6}$$

Here, E is Young's modulus, ν is Poisson's ratio and E_s is the ratio of stress and strain for the elastic uniaxial Kirchhoff stress vs natural strain curve. Introducing the effective Poisson's ratio ν_s

$$\nu_s = \frac{1}{2} + \frac{E_s}{E}\left(\nu - \frac{1}{2}\right) \tag{2.7}$$

the relation (2.6) can be rewritten as

$$\varepsilon_i = \frac{1+v_s}{E_s}\tau_i - \frac{v_s}{E_s}(\tau_1+\tau_2+\tau_3) \tag{2.8}$$

and the inverted form is

$$\tau_i = \frac{E_s}{1+v_s}\left[\varepsilon_i + \frac{v_s}{1-2v_s}(\varepsilon_1+\varepsilon_2+\varepsilon_3)\right]. \tag{2.9}$$

For this material a strain energy function $\Phi = \Phi(\varepsilon_1, \varepsilon_2, \varepsilon_3)$ can be constructed such that $\tau_i = \partial\Phi/\partial\varepsilon_i$.

On the fixed current principal stress axes, Hill (1969, 1970, 1978) has shown that the Jaumann rate of Kirchhoff stress $\overset{\nabla}{\tau}_{ij}$ is related to the Eulerian strain-rate $\dot{\varepsilon}_{ij}$ by

$$\overset{\nabla}{\tau}_{ij} = \frac{\partial\tau_i}{\partial\varepsilon_1}\dot{\varepsilon}_{11} + \frac{\partial\tau_i}{\partial\varepsilon_2}\dot{\varepsilon}_{22} + \frac{\partial\tau_i}{\partial\varepsilon_3}\dot{\varepsilon}_{33} \quad (\text{for } i = 1,2,3; \text{no sum}) \tag{2.10}$$

$$\overset{\nabla}{\tau}_{ij} = \frac{\lambda_i^2+\lambda_j^2}{\lambda_i^2-\lambda_j^2}(\tau_i-\tau_j)\dot{\varepsilon}_{ij} \quad (\text{for } i \neq j; \text{no sum}) \tag{2.11}$$

where λ_i are the principal stretches and $\varepsilon_i = \ln(\lambda_i)$.

On the principal axes, the relation between the Jaumann derivative of Kirchhoff stress $\overset{\nabla}{\tau}_{ij}$ and the Eulerian strain-rate $\dot{\varepsilon}_{ij}$ is written as

$$\overset{\nabla}{\tau}_{ij} = R_{ijkl}\dot{\varepsilon}_{kl} \tag{2.12}$$

where the components for $i = j$ and $k = l$ are obtained directly from differentiation in (2.9). The shear moduli are obtained from (2.11), using (2.9), to give

$$R_{1212} = R_{2112} = R_{1221} = R_{2121} = \frac{E_s}{2(1+v_s)}(\varepsilon_1-\varepsilon_2)\coth(\varepsilon_1-\varepsilon_2), \text{etc.} \tag{2.13}$$

The finite strain elastic relations (2.6–2.13) can be used to represent a wide class of nonlinear elastic stress-strain curves, by using appropriate choices of the function E_s. However, in the present paper $E_s = E$ will be chosen, and thus also $v_s = v$ according to (2.7).

For the finite strain analyses here, a Lagrangian convected coordinate formulation of the field equations is adopted, in which a material point is identified by the coordinates x^i in the reference frame and the displacement components u^i on the reference base vectors. The metric tensors in the current configuration and the reference configuration are denoted by G_{ij} and g_{ij}, respectively, with determinants G and g, and the contravariant components of the Kirchhoff stress tensor τ^{ij} and the Cauchy stress tensor σ^{ij} are related by $\tau^{ij} = \sqrt{\mathrm{G}/\mathrm{g}}\sigma^{ij}$. Latin indices range from 1 to 3, and the summation convention is used for repeated indices.

For use in the Lagrangian formulation the components of the tensor $\mathbf{R}$ on the embedded deformed coordinates are computed. It is convenient to first transform the relations (2.12) to the fixed, global, Cartesian coordinate system, $\overset{\nabla}{\boldsymbol{\tau}} = \mathbf{R}:\mathbf{D}$, and then transforming these relations to deformed base vectors

$$\overset{\nabla}{\tau}{}^{ij} = R^{ijkl}\dot{\eta}_{kl} \tag{2.14}$$

using the relations $R^{ijkl} = \mathbf{R}(\cdot\bar{\mathbf{e}}^i)\,(\cdot\bar{\mathbf{e}}^j)\,(\cdot\bar{\mathbf{e}}^k)\,(\cdot\bar{\mathbf{e}}^l)$, $\tau^{ij} = \bar{\mathbf{e}}^j = \boldsymbol{\tau}\cdot\bar{\mathbf{e}}^j$ and $\dot{\eta}_{ij} = \bar{\mathbf{e}}_i\cdot\mathbf{D}\cdot\bar{\mathbf{e}}_j$. Here, the current base vectors $\bar{\mathbf{e}}_i$ are given in terms of the reference base vectors $\mathbf{e}_j$ by

$$\bar{\mathbf{e}}_i = (\mathrm{g}_{ij} + u_{j,i})\mathbf{e}^j. \tag{2.15}$$

It is noted that the Jaumann derivatives in (2.10–2.12), and thus also (2.14), result from differentiation of the elastic relationships (2.9), and therefore this stress rate is corotational with the elastic spin rate. However, the plasticity description to be used here is J_2 flow theory with isotropic hardening, for which the plastic spin is taken to be zero, $\mathbf{W}^p \equiv \mathbf{0}$, as mentioned below (2.4–2.5). Therefore, in the present case, the Jaumann rate in (2.14) is also corotational with the total spin rate.

2.3. Elastic–plastic constitutive relations

In J_2 flow theory, based on the Mises yield condition, the plastic part of the strain rate is of the form $\dot{\eta}^p_{ij} = \dot{\lambda} s_{ij}$. Here, the Mises stress is $\sigma_e = (3s_{ij}s^{ij}/2)^{1/2}$, with the stress deviator $s^{ij} = \tau^{ij} - G^{ij}\tau^k_k/3$, and for a hardening material the parameter $\dot{\lambda}$ is proportional to the Mises stress rate, $\dot{\sigma}_e = (3/2\sigma_e)s_{kl}\overset{\nabla}{\tau}{}^{kl}$. Then, the expression for the plastic part of the strain rate can be written on the form

$$\dot{\eta}^p_{ij} = \frac{1}{H}\mathrm{m}_{ij}\,\mathrm{m}_{kl}\overset{\nabla}{\tau}{}^{kl}, \quad \mathrm{m}_{ij} = \frac{3}{2}\frac{s_{ij}}{\sigma_e} \tag{2.16}$$

The value of the hardening parameter H is found by using $\dot{\eta}_{ij} = \dot{\eta}^e_{ij} + \dot{\eta}^p_{ij}$ together with the assumption in the present paper that $E_s = E$ (see below (2.13)). Then, with E_t denoting the slope of the uniaxial Kirchhoff stress vs natural strain curve, the expression for H is

$$H = \frac{EE_\mathrm{t}}{E - E_\mathrm{t}}. \tag{2.17}$$

If a fully nonlinear elasticity description was used instead, with a function $E_s(\sigma_e)$ in (2.6–2.13), this would affect (2.17). Then, Young's modulus E in (2.17) would have to be replaced by the slope E^*_t of the elastic uniaxial Kirchhoff stress vs natural strain curve at the current stress level.

In the presence of plastic deformations the elastic relationship (2.14) takes the form $\overset{\nabla}{\tau}{}^{ij} = R^{ijkl}(\dot{\eta}_{kl} - \dot{\eta}^p_{kl})$, which can be rewritten as

$$\overset{\nabla}{\tau}{}^{ij} = (R^{ijkl} - \mu M^{ij}M^{kl})\dot{\eta}_{kl}, \quad M^{ij} = R^{ijrs}\,m_{rs} \tag{2.18}$$

$$\mu = \begin{cases} 0, & \text{for } \sigma_e < (\sigma_e)_{\max} \quad \text{or } \dot{\sigma}_e < 0 \\ [H + m_{rs}M^{rs}]^{-1}, & \text{for } \sigma_e = (\sigma_e)_{\max} \quad \text{and } \dot{\sigma}_e > 0 \end{cases} \tag{2.19}$$

From (2.18) the incremental constitutive relations on the standard form $\dot{\tau}^{ij} = L^{ijkl}\dot{\eta}_{kl}$ are obtained directly.

In the description given above, the elastic constitutive relations are first written on principal stress axes (2.12), then transformed to the current deformed base vectors (2.14), and finally combined with the plastic strain rate expression (2.16) on current deformed base vectors, to give the incremental elastic–plastic constitutive relations (2.18). Alternatively, the plastic strain rate

expression can be specified on the principal stress axes and combined with (2.12) to give the incremental elastic–plastic constitutive relations on the principal stress axes. Subsequently these relations can then be transformed to the current deformed base vectors, to be used in the numerical solution. It is noted that both methods have been used int he present computations, and it has been checked that they give identical results.

The uniaxial Kirchhoff stress vs natural strain curve is represented by a piecewise power hardening law of the form

$$\tau = \begin{cases} E\varepsilon, & \text{for } \tau < \sigma_Y \\ \sigma_y \left(\dfrac{\varepsilon}{\varepsilon_Y}\right)^{\mathrm{N}}, & \text{for } \tau \geqslant \sigma_Y \end{cases} \tag{2.20}$$

where $\varepsilon_Y = \sigma_Y/E$ is the initial yield strain, σ_Y is the initial yield (Kirchhoff) stress, and N is the strain-hardening exponent. It is noted that the use of a constant E in (2.20a) is a direct result of the assumption in the present paper that $E_s = E$ in (2.6–2.13).

3. Problem for formulation and numerical method

Analyses of the growth of a single void in an infinite solid can be carried out by coupling an analytical solution for an outer region to a numerical finite strain solution for an inner region (Huang et al., 1991; Tvergaard et al., 1992). In a study of the effect of initial ellipsoidal void shapes on cavitation instabilities Tvergaard and Hutchinson (1993) have preferred using a finite element approximation in the whole region analysed, thus considering a cylindrical cell model with a central void. This cylindrical cell model has been used (Tvergaard, 1982; Hutchinson and Tvergaard, 1989) to represent a periodic distribution of voids, but with a sufficiently small void volume fraction of about 2.5×10^{-11} it was found that the studies gave a very good approximation of the behaviour of a single void in an infinite solid (Tvergaard and Hutchinson, 1993).

In the present analyses the cylindrical unit cell is used. The initial dimensions of the cell are specified by the height H_0 in the axial direction, the outer radius B_0 and the void radius R_0. A cylindrical reference coordinate system is used, in which x^1 is the axial coordinate, x^2 is the radial coordinate, and x^3 is the circumferential angle. In terms of the displacement components u^i on the reference base vectors and the nominal surface tractions T^i, the boundary conditions for the unit cell are, on incremental form,

$$\dot{u}^1 = 0, \quad \dot{T}^2 = \dot{T}^3 = 0, \quad \text{at } x^1 = 0 \tag{3.1}$$

$$\dot{u}^1 = \dot{U}_{\mathrm{I}}, \quad \dot{T}^2 = \dot{T}^3 = 0, \quad \text{at } x^1 = \mathrm{H}_0 \tag{3.2}$$

$$\dot{u}^2 = \dot{U}_{\mathrm{II}}, \quad \dot{T}^1 = \dot{T}^3 = 0, \quad \text{at } x^2 = \mathrm{R}_0 \tag{3.3}$$

$$\dot{T}^i = 0, \quad \text{at} (x^1)^2 + (x^2)^2 = R_0^2. \tag{3.4}$$

The two constants $\dot{U}_{\mathrm{I}}$ and $\dot{U}_{\mathrm{II}}$ are displacement increments and the ratio $\dot{U}_{\mathrm{II}}/\dot{U}_{\mathrm{I}}$ is calculated in each increment such that there is a fixed prescribed ratio $\rho = T/S$, between the macroscopic true

stresses (see Tvergaard, 1982). Here, S is the average true stress in the axial direction, while T is the average true stress in the radial directions.

Constitutive relations and equilibrium equations are specified here in the context of convected coordinate formulation of the field equations. The Lagrangian strain tensor is expressed in terms of the displacement components as

$$\eta_{ij} = \frac{1}{2}(u_{i,j} + u_{j,i} + u^k_{,i} u_{k,j}) \tag{3.5}$$

where $(\,)_{,j}$ denoted covariant differentiation in the reference frame.

The equations of equilibrium are expressed in terms of the principle of virtual work, and a numerical solution is obtained by a linear incremental solution procedure. The equations governing the stress increments $\Delta\tau^{ij}$, the strain increments $\Delta\eta_{ij}$, etc., are obtained by expanding the principle of virtual work about the current state, using (3.5). To lowest order the incremental equation is

$$\int_V \{\Delta\tau^{ij}\delta\eta_{ij} + \tau^{ij}\Delta u^k_{,i}\delta u_{k,j}\}\,\mathrm{d}\,V = \int_A \Delta T^i \delta u_i\,\mathrm{d}\,A - \left[\int_V \tau^{ij}\delta\eta_{ij}\,\mathrm{d}\,V - \int_A T^i\delta u_i\,\mathrm{d}\,A\right] \tag{3.6.}$$

where V and A are the volume and surface, respectively, of the body in the reference configuration and T^i are contravariant components of the nominal surface tractions. The bracketed terms are included to prevent drifting of the solution away from the true equilibrium path.

The displacement fields are approximated in terms of axisymmetric 8-noded isoparametric elements, as in Tvergaard (1982). The volume integral in (3.6) is carried out by using 2×2 point Gauss integration (i.e. reduced integration) within each element. An example of a mesh used for the analyses is shown in Fig. 1, illustrating both the outer mesh in the unit cell and the central part of the mesh near a spherical void.

A special Rayleigh–Ritz finite element method (Tvergaard, 1976) is used to be able to prescribe a node displacement at the void surface rather than the end displacement U_1 without applying a

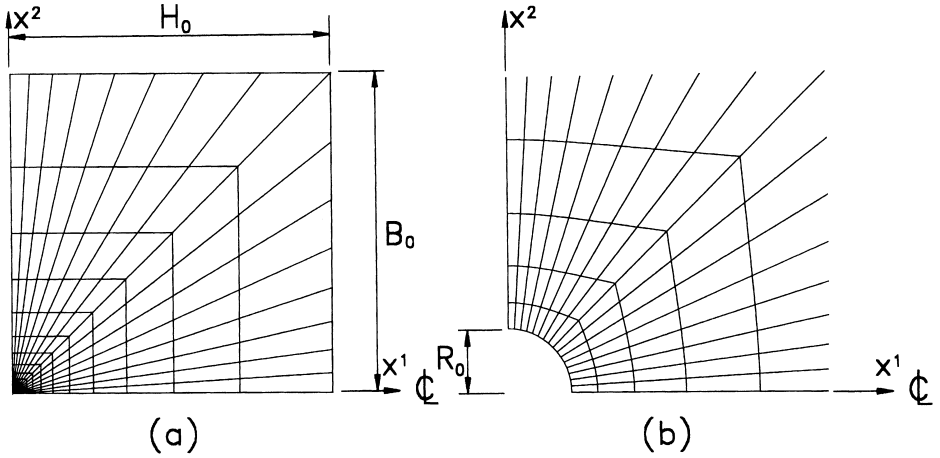

Fig. 1. Mesh used for numerical analyses. (a) The axisymmetric unit cell. (b) Inner mesh near the void.

load on the void surface. This improves the numerical stability near the occurrence of a cavitation instability where $\dot{U}_I \to 0$.

4. Results

In the first case to be analysed the material is taken to be power hardening with $N = 0.1$, Poisson's ratio is $\nu = 0.3$, and various values of the initial yield strain σ_Y/E are considered. The initial dimensions of the unit cell analysed are specified by $H_0/B_0 = 1$ and $R_0/B_0 = 0.001$, so that the initial void volume fraction in the cell is 6.7×10^{-10}. The computations are carried out with a mesh consisting of 20×16 elements, as shown in Fig. 1. It is noted that comparisons with analyses using only 10 elements in the radial direction have shown very small mesh sensitivity. Also, comparison with results obtained for $R_0/B_0 = 0.01$ show little sensitivity to the void size, so that the void volume fraction used in the present cell model studies is small enough to represent a single void in an infinite solid.

Figure 2 gives results for a material subject to remote hydrostatic tension, $\rho = T/S = 1$. The curves show the development of axial stress S vs void volume V, normalized by σ_Y and the initial void volume V_0, respectively, with V/V_0 given on a logarithmic scale. The remote stress level for the cavitation instability is reached when the slope of these curves becomes zero, which appears to occur somewhere around $V/V_0 = 100$ for the curves in Fig. 2. After that the maximum macroscopic stress has been reached, this stress remains constant during a large amount of subsequent void growth, which confirms that the initial void volume has been chosen small enough to adequately represent an infinite solid. If the initial void volume fraction had been too large, the stress S would clearly decay after reaching the maximum, as is well known from previous cell model studies of void growth (e.g. see Tvergaard, 1982). The computations in Fig. 2 are stopped at values of V/V_0 slightly below 1000, since here the mesh near the void is so distorted that the solution breaks down

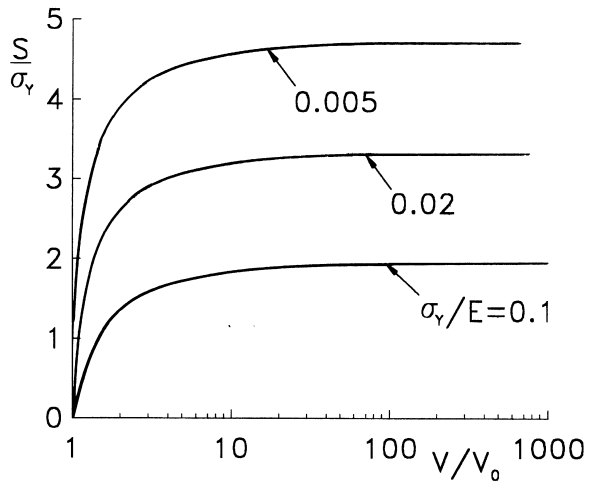

Fig. 2. Remote axial stress vs void volume for $T/S = 1$, $N = 0.1$ and $\nu = 0.3$.

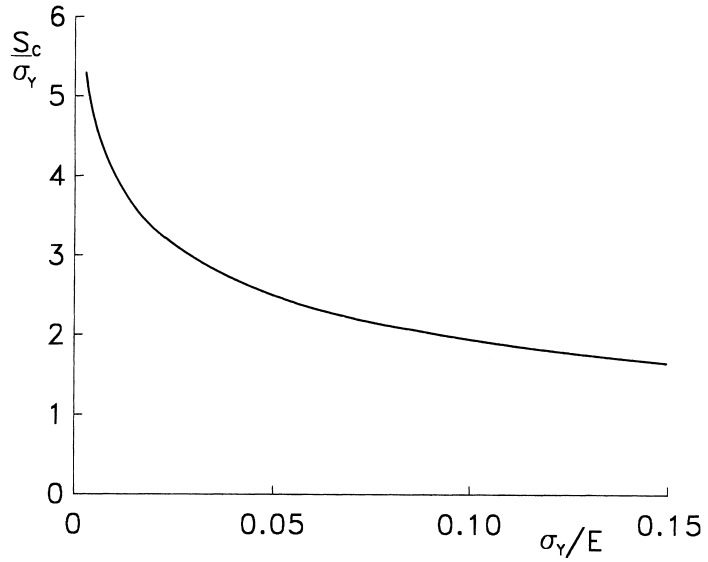

Fig. 3. Critical stress for cavitation instability vs initial yield strain, for $T/S = 1$, $N = 0.1$ and $\nu = 0.3$.

numerically. If remeshing had been used, such computations could be continued to much larger values of V/V_0 (Tvergaard, 1997).

The three curves in Fig. 2 show the expected effect that the critical cavitation stress, S_c/σ_Y, decays strongly as the initial yield strain, σ_Y/E, is increased. The value $\sigma_Y/E = 0.005$ is in the range relevant to metal plasticity, and here the critical stress is high, $S_c/\sigma_Y = 4.71$, as found by Huang et al. (1991). But the critical stress values $S_c/\sigma_Y = 3.32$ for $\sigma_Y/E = 0.02$ and $S_c/\sigma_Y = 1.95$ for $\sigma_Y/E = 0.1$ illustrate the strong sensitivity to the initial yield strain. Based on a number of computations of the type shown in Fig. 2 the critical stress values for a large range of σ_Y/E values, between 0.003 and 0.15, are given in Fig. 3.

In relation to the finite strain description (2.6–2.14) used here for the elastic part of the deformations, it is of interest to note that for $\rho = 1$ the void growth problem in an infinite solid is a spherically symmetric problem. Then, in any material point, the principal stress axes remain fixed relative to the material, along the radius and two transverse directions, and this means that the shear moduli (2.13) are never active in the problem solution. Then, since these shear moduli are the only difference from the hypoelastic moduli (see Tvergaard et al., 1981), the full elastic–plastic solution will not differ from that based on using the hypoelastic model. With the present cylindrical cell model, there is not complete spherical symmetry, but spherical symmetry is so well approximated in most of the cell that the difference hardly matters. It should be emphasized though that even for spherically symmetric conditions there is not proportional stressing, as discussed by Tvergaard et al. (1992), and therefore predictions based on the finite strain J_2-flow theory are expected to differ from predictions based on the corresponding J_2-deformation theory. Thus, for a material point at the onset of plastic flow the condition $\tau_R = \tau_\theta - \sigma_Y$ is satisfied, where τ_R and τ_θ are the radial and transverse principal stresses, respectively. But after that this material point has

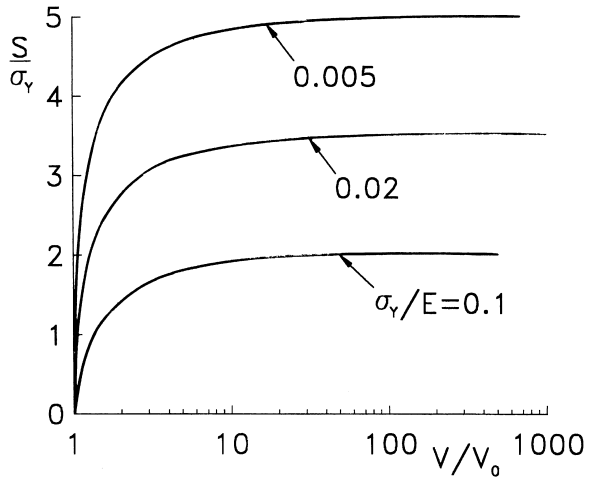

Fig. 4. Remote axial stress vs void volume for $T/S = 0.9$, $N = 0.1$ and $v = 0.3$.

been engulfed in the plastic zone around the expanding void and has effectively reached the void surface, the radial principal stress is $\tau_R = 0$, while τ_θ is well above σ_Y.

For $\rho = 0.9$ the curves in Fig. 4 show the development of axial stress S vs void volume V, analogous to the curves in Fig. 2 for $\rho = 1$. The reductions in the critical cavitation stress for increasing values of the initial yield strain are very similar to those found for $\rho = 1$. Also, for all three curves the critical axial stress S_c is higher when $\rho = 0.9$, but the difference from the curves in Fig. 2 is quite small at the largest initial yield strain, $\sigma_Y/E = 0.1$, where $S_c/\sigma_Y = 2.01$ in Fig. 4. Again, it is noted that the critical stress level is reached somewhere in the range around $V/V_0 = 100$, a bit earlier for the higher value of σ_Y/E.

The effect of the strain hardening level was investigated by Huang et al. (1991) for remote hydrostatic loading and by Tvergaard et al. (1992) for other axisymmetric stress states. It was found in these investigations for low values of σ_Y/E that the critical stress level depends rather strongly on the strain hardening, such that the critical stress is much higher for a high hardening material, presuming that the values of other material parameters are unchanged. For the much higher initial yield strain, $\sigma_Y/E = 0.1$, and for $\rho = 0.9$, Fig. 5 shows a comparison between the axial stress vs void volume growth curves for three different levels of strain hardening. Here, the curve for $N = 0.1$ is identical to one of the curves in Fig. 4. It is seen that increased strain hardening still gives an increased critical stress level for the onset of a cavitation instability, but the dependence is much less pronounced than that found in the earlier studies for low values of σ_Y/E.

In Fig. 6 the critical stress values for $\rho = 0.9$ are shown as functions of σ_Y/E for the three different values of the strain hardening exponent considered in Fig. 5. The values of σ_Y/E range from 0.002 to 0.15. The curve for $N = 0.1$ in Fig. 6 is directly comparable to the curve in Fig. 3, and it is seen that the critical axial stress S_c is larger for $\rho = 0.9$ than for $\rho = 1$, in the whole range considered. Regarding the effect of different levels of strain hardening, it is noted that at $\sigma_Y/E = 0.005$, the value of S_c is increased by 48% when the strain hardening exponent N is increased from 0.05 to 0.2, whereas at $\sigma_Y/E = 0.15$ the corresponding increase is only 14%.

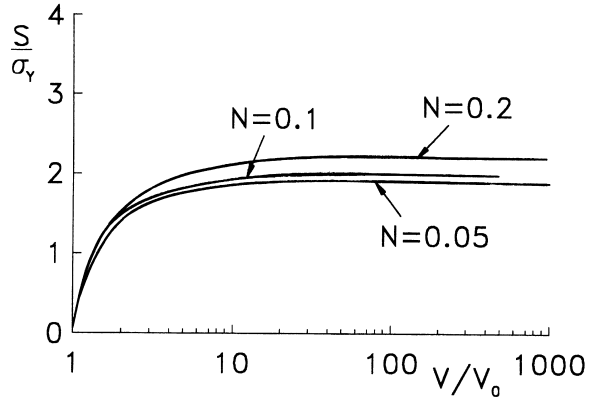

Fig. 5. Remote axial stress vs void volume for $T/S = 0.9$, $\sigma_Y/E = 0.1$ and $\nu = 0.3$.

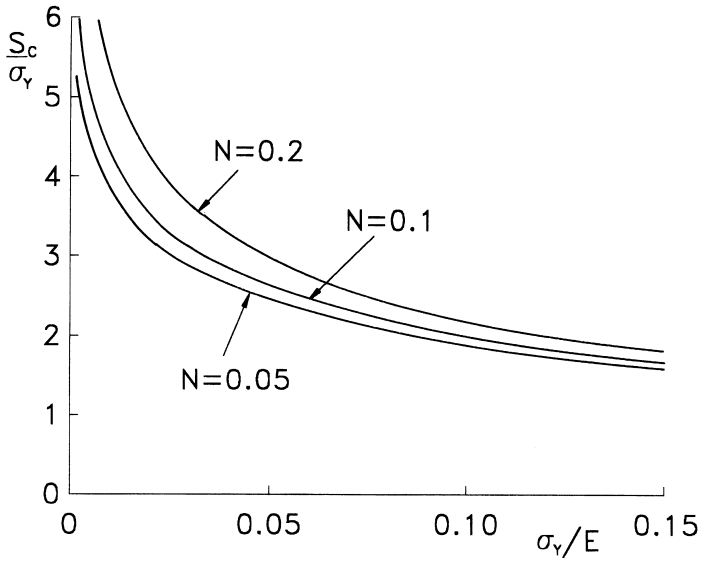

Fig. 6. Critical stress for cavitation instability vs initial yield strain for $T/S = 0.9$ and $\nu = 0.3$.

The dependence on Poisson's ratio was considered briefly by Huang et al. (1991), mainly because their numerical studies were carried out for $\nu = 0.3$, while a number of simple model studies for spherically symmetric conditions were carried out for incompressible elastic material behaviour, $\nu = 0.5$. In fact, spherically symmetric results given by Huang et al. (1991) for incompressible elastic–plastic material are also valid for large elastic strains. It was found by Huang et al. (1991) that the values of S_c are somewhat higher for higher values of ν. In Fig. 7 the dependence of ν is illustrated for $\sigma_Y/E = 0.1$, $N = 0.1$ and $\rho = 0.9$. The dependence on ν appears to be close to linear in the range investigated, and it is seen that incompressible elastic response will give rise to somewhat higher values of S_c than those shown in the previous figures, for $\nu = 0.3$,

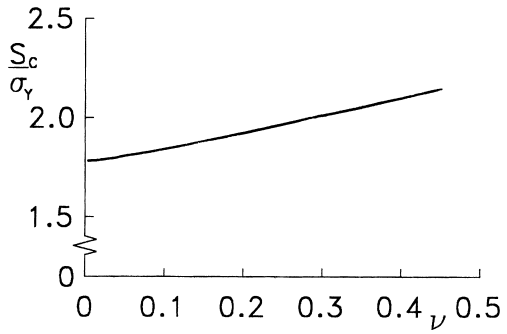

Fig. 7. Critical stress for cavitation instability vs the value of Poisson's ratio, for $T/S = 0.9$, $\sigma_Y/E = 0.1$ and $N = 0.1$.

In the general case, for $\rho \neq 1$, such as the solutions illustrated in Figs 4–7, the principal stress directions rotate relative to the material during the deformation process, and therefore the solutions are dependent on using the shear moduli (2.13), corresponding to the truly elastic material description. Comparison with predictions based on the standard hypoelastic expressions for the elastic moduli show differences in the values of the moduli. However, for the cases studied here, the rotations of the principal stress axes are not very dominant, so the values of stress and strain quantities predicted by the two approaches differ only a little in the cases where comparison has been carried out. Furthermore, it is noted that the value of the expression $\Delta\varepsilon \coth(\Delta\varepsilon)$ in (2.13) is 1.003 for $\Delta\varepsilon = 0.1$, 1.030 for $\Delta\varepsilon = 0.3$, and 1.082 for $\Delta\varepsilon = 0.5$, which indicates that the deviation from unity grows only rather slowly with increasing strain level. Therefore, the elastic strain levels considered in the present paper are not large enough to give a significant difference from predictions based on using the hypoelastic expressions.

5. Discussion

The present studies of cavitation instabilities have focused on the effect of a large initial yield strain for a power hardening elastic–plastic material. Extrapolation of results by Huang et al. (1991) already indicate that the cavitation stress will be much reduced when the value of σ_Y/E is increased. However, the type of analyses carried out here are necessary to obtain quantitative information. To properly account for the rather large elastic strains occurring here, the elastic part of the deformation is represented in terms of a truly elastic (hyperelastic) material description, rather than the hypoelastic approximation of elastic deformations often used in metal plasticity.

The large values of the initial yield strain considered here are unrealistic for metals. Therefore, the present investigation is inspired by other materials, such as polymers, which show an elastic–plastic type of behaviour with high values of σ_Y/E. However, the material model applied here does not attempt to make use of the special descriptions developed by various authors for the inelastic deformation of polymers. While retaining classical plasticity, the interest here is devoted to the effect of the initial yield strain varying over a large range of values, as most clearly illustrated by the curves in Figs 3 and 6. It is noted that some of the interest in void growth for polymers relates to polymer–rubber blends, where the voids are often formed as a result of cavitation within the

rubber particles. In such cases, for initial void radii much smaller than the outer radius of the rubber particle, an initial cavitation instability will be governed by rubber elasticity, and polymer plasticity will start to play a role when the void radius is closer to the current radius of the rubber inclusions. The present studies have no such effect of rubber elasticity, so here the effect of the non-proportional loading path affects the solution from the early onset of cavity growth, as has been discussed in relation to the results in Figs 2 and 3.

The effect of strain rate dependent yielding is not considered in the present paper, but such effects would be important for materials such as polymers. Abeyaratne and Hou (1989) have studied instabilities of cavity growth in a rate-dependent solid for spherically symmetric conditions with incompressible material behaviour. They study a variety of rate-dependent material laws and distinguish between stress levels where cavity growth is slow and levels where growth is fast, but the general conclusion is that for the most common class of visco-plastic materials the void will grow without bound at any tensile stress level. In the rate-independent limit of the material considered the behaviour reduces to the known cavitation instability behaviour for the corresponding rate-independent material.

As shown in Figs 5 and 6, a more high hardening material results in a higher critical stress for cavitation, as was also found by Tvergaard et al. (1992). However, the relative increase of the cavitation stress is much smaller at the high values of the initial yield strain considered here than was found at small values of the yield strain. The influence of Poisson's ratio for the elastic part of the deformation is shown in Fig. 7 to be rather weak, but the tendency is that the incompressible elastic material behaviour will result in a slightly higher critical stress for cavitation.

The effect of using the truly elastic material description is found to be small in the cases studied here, seen in relation to predictions based on the corresponding hypoelastic model. For spherically symmetric conditions, where the principal stress directions do not rotate relative to the material, there is no difference at all. But also in the more general axisymmetric cases analysed the differences are quite small.

References

Abeyaratne, R., Hou, H.-S., 1989. Growth of an infinitesimal cavity in a rate-dependent solid. J. Appl. Mech., Transactions of the ASME 56, 40–46.

Arruda, E.M., Boyce, M.C., 1991. Evolution of plastic anisotropy in amorphous polymers during finite straining. In: Boehler, J.-P., Khan, A.S. (Eds.), Anisotropy and Localization of Plastic Deformation. Elsevier Applied Science, London, pp. 483–488.

Ashby, M.F., Blunt, F.J., Bannister, M., 1989. Flow characteristics of highly constrained metal wires. Acta Metallurgic 37, 1857.

Ball, J.M., 1982. Discontinuous equilibrium solutions and cavitation in nonlinear elasticity. Phil. Trans. R. Soc. London A306, 557–610.

Bishop, R.F., Hill, R., Mott, N.F., 1945. The theory of indentation and hardness tests. Proc. Phys. Soc. 57, 147–159.

Boyce, M.C., Parks, D.M., Argon, A.S., 1988. Large inelastic deformation of glassy polymers, Part I: rate dependent constitutive model. Mech. Mater. 7, 15–33.

Hill, R., 1950. The Mathematical Theory of Plasticity. Clarendon Press, Oxford.

Hill, R., 1969. Some aspects of the incremental behaviour of isotropic elastic solids after finite strain. In: Sedov, L.I. et al. (Eds.), Problems in Mechanics: Deformation of Solid Bodies. (V.V. Novozhilov 60th Anniversary Volume), (in Russian). Izdat, Sudostroenie, Leningrad, p. 459.

Hill, R., 1970. Constitutive inequalities for isotropic elastic solids under finite strain. Proc. Roy. Soc. London, A314, 457.

Hill, R., 1978. Aspects of invariance in solid mechanics. In: Yih, C.-S. (Ed.), Advances in Applied Mechanics 18, 1, Academic Press, New York.

Horgan, C.O., 1992. Void nucleation and growth for compressible nonlinearly elastic materials: an example. Int. J. Solids Structures 29, 279–291.

Horgan, C.O., Abeyaratne, R., 1986. A bifurcation problem for a compressible nonlinearly elastic medium: growth of a microvoid. J. Elasticity 16, 189–200.

Huang, Y., Hutchinson, J.W., Tvergaard, V., 1991. Cavitation instabilities in elastic–plastic solids. J. Mech. Phys. Solids 39, 223–241.

Hutchinson, J.W., 1973. Finite strain analysis of elastic–plastic solids and structures. In: Hartung, R.F. (Ed.), Numerical Solution of Nonlinear Structures Problems 17–29, ASME, New York.

Hutchinson, J.W., Neale, K.W., 1978. Sheet necking–II. Time–independent behavior. In: Koistinen, D.P., Wang, N.-M. (Eds.), Mechanics of Sheet Metal Forming. Plenum, p. 127.

Hutchinson, J.W., Tvergaard, V., 1980. Surface instabilities on statically strained plastic solids. Int. J. Mech. Sci. 22, 339–354.

Hutchinson, J.W., Tvergaard, V., 1981. Shear band formation in plane strain. Int. J. Solids Structures 17, 451–470.

Hutchinson, J.W., Tvergaard, V., 1989. Softening due to void nucleation in metals. In: Wei, R.P., Gongloff, R.P. (Eds.), Fracture Mechanics: Perspective and Directions, ASTM STP 1020. American Society for Testing and Materials, Philadelphia, pp. 61–83.

Needleman, A., 1985. On finite element formulations for large elastic–plastic deformations. Computers & Structures 20, 247–257 .

Steenbrink, A.C., van der Giessen, E., 1997. Void growth in glassy polymers: effect of yield properties on hydrostatic expansion. Int. J. Damage Mech. 6, 317–330.

Tvergaard, V., 1976. Effect on thickness inhomogeneities in internally pressurized elastic–plastic spherical shells. J. Mech. Phys. Solids 24, 291–304.

Tvergaard, V., 1982. On localization in ductile materials containing spherical voids. Int. J. Fracture 18, 237–252.

Tvergaard, V., 1996. Effect of void size difference on growth and cavitation instabilities. J. Mech. Phys. Solids 44, 1237–1253.

Tvergaard, V., 1998. Interaction of very small voids with larger voids. J. Mech. Phys. Solids 35, 3989–4000.

Tvergaard, V., 1997. Studies of void growth in a thin ductile layer between ceramics. Computational Mech. 20, 186–191.

Tvergaard, V., Hutchinson, J.W., 1993. Effect of initial void shape on the occurrence of cavitation instabilities in elastic–plastic solids. J. of Appl. Mech. 60, 807–812.

Tvergaard, V., Needleman, A., Lo, K.K., 1981. Flow localization in the plane strain tensile test. J. Mech. Phys. Solids 29, 115–142.

Tvergaard, V., Huang, Y., Hutchinson, J.W., 1992. Cavitation instabilities in a power hardening elastic–plastic solid. Eur. J. Mech., A/Solids 11, 215–231.

Wu, P.D., van der Giessen, E., 1993. On improved network models for rubber elasticity and their applications to orientation hardening in glassy polymers. J. Mech. Phys. Solids 41, 427–456.